

Contents lists available at ScienceDirect

Chemical Engineering Journal

journal homepage: www.elsevier.com/locate/cej





Ru decorated Co nanoparticles supported by *N*-doped carbon sheet implements Pt-like hydrogen evolution performance in wide pH range

Dengke Zhao a , Zilong Li b , Xiaolong Yu b , Wei Zhou a , Qikai Wu a , Yun Luo e , Nan Wang c , Anmin Liu d , Ligui Li a , Shaowei Chen f

- ^a Guangzhou Key Laboratory for Surface Chemistry of Energy Materials, New Energy Research Institute, School of Environment and Energy, South China University of Technology, Guangzhou Higher Education Mega Center, Guangzhou 510006, China
- b Guangdong Provincial Key Laboratory of Petrochemical Pollution Processes and Control, School of Environmental Science and Engineering, Guangdong University of Petrochemical Technology, Maoming, Guangdong 525000, China
- ^c Siyuan Laboratory, Guangzhou Key Laboratory of Vacuum Coating Technologies and New Energy Materials, Department of Physics, Jinan University, Guangzhou, Guangdong 510632, China
- d State Key Laboratory of Fine Chemicals, School of Chemical Engineering, Dalian University of Technology, China
- e Nanobio Spectroscopy Team, LCBPT CNRS UMR 8601, Université de Paris, 75006 Paris, France
- f Department of Chemistry and Biochemistry, University of California, 1156 High Street, Santa Cruz, CA 95064, United States

ARTICLE INFO

Keywords: Hydrogen evolution reaction pH-universal Electrocatalyst Ru-Co heterostructure

ABSTRACT

Development of high-performance pH-universal electrocatalyst for hydrogen evolution reaction (HER) is a vital step towards hydrogen economy but remains a major challenge. Herein, the Ru decorated Co nanoparticles supported by N-doped carbon sheets (Ru/Co@NC) are prepared by galvanic exchange reaction and display a remarkable performance for HER. In the 1.0 M KOH, 0.01 M PBS and 0.5 M H_2SO_4 , respectively, Ru/Co@NC shows low overpotentials of 10, 283 and 50 mV at the current density of 10 mA cm⁻², comparable to benchmark Pt/C (23, 289 and 37 mV). Furthermore, deep experimental researches and DFT calculations indicate that the Ru-Co heterostructure shows more suitable energy of H_2O^* dissociation and H^* adsorption compared to Ru and Co, which can significantly improve the HER activity. Besides excellent activity, in a wide pH range, the Ru/Co@NC also exhibits good stability with negligible current loss after a long-time HER test (30 h). This work may provide ponderable strategies for developing an efficient pH-universal HER electrocatalyst.

1. Introduction

Hydrogen (H₂) with high energy density (142.4 kJ kg⁻¹) and carbon neutrality is considered the most promising energy carrier to replace the traditional fossil energy in the future and attracted more and more attention[1–3]. Electrocatalytic water splitting (EWS) is one of the most sustainable routes to generate clean H₂ among the many hydrogen production technologies, which can be powered by renewable energy like tidal, solar and wind[4–6]. In order to lift the conversion efficiency of EWS, efficient electrocatalysts are often applied to reduce the overpotential (η) of hydrogen/oxygen evolution reaction (H/OER)[7–10]. Currently, foremost HER electrocatalysts are platinum (Pt) and its derivatives, but the low abundance and exorbitant price impede the large-scale applications[11]. Moreover, owing to the higher water dissociation energy (H₂O + e[·] + * \rightarrow OH⁻ + H*), Pt-based noble metals show 2 or

3 orders of magnitude slower reaction kinetics in alkaline or neutral environments [12], further limiting the widespread harvesting of $\rm H_2$. To date, numerous studies have been focused on the earth-abundant alternatives as the efficient electrocatalysts for HER and achieved remarkable results [13–16]. Yet low intrinsic activity makes them still unable to compare benchmark Pt/C, and the stability tends to degrade in a wide pH range. Hence, it is critical but challenging to explore cheap and pH-universal HER catalysts with high activity and stability.

To balance activity and cost, other cheaper Pt-group mental such as Ru and its derivatives have been attracting more and more attention in the last decade owing to the high catalytic activity for HER[17–21]. For example, numerous studies have shown that the N-doped carbon supported Ru nanoparticles (NPs) catalysts (Ru/C) such as Ru-ENG[22], Ru-NG[23] and Ru/C₃N₄/C[24] display Pt-like HER activity at wide pH because of the suitable hydrogen adsorption/desorption energy. Despite

E-mail addresses: nanwang@email.jnu.edu.cn (N. Wang), liuanmin@dlut.edu.cn (A. Liu), esguili@scut.edu.cn (L. Li).

^{*} Corresponding authors.

good progress having been made, the activity and stability of the reported Ru/C-based HER electrocatalysts are still far from being desired on account of the inevitable agglomeration and dissolution of Ru during the electrocatalytic process. Optimizing the carbon-based substrate to enhance the support-metal interaction is a reliable strategy to improve electrocatalytic HER activity and stability[25]. Compared to N-dopedcarbon, transition metal embedded N-doped carbon (TM@NC, TM = Fe, Co or Ni) is more ideal supports, because TM in TM@NC not only can change the filling level of Ru d-band, but also can anchor Ru to boost support-metal interaction[26-30], which is conducive to enhance the performance and stability. In addition, the structure of carbon substrate also plays a crucial part in catalytic activity. In this case, 2D porous carbon nanostructures with the excellent aperture structure and specific surface area are the most explored because the exposure of active sites can be maximized[31]. However, the traditional 2D carbon-based materials, like graphene, tend to aggregate or restack during the synthesis on account of the strong Van der Waals interaction between adjacent layers, resulting in reduced electrocatalytic performance[32]. So, reasonable integration of 2D TM@NC and Ru is an effective approach to prepare pH-universal HER catalysts with high performance.

Herein, the Ru decorated Co nanoparticles supported by *N*-doped carbon sheets (Ru/Co@NC) have been prepared using g-C₃N₄ as thermally removable 2D templates for the substrate formation and through galvanic replacement. A series of characterizations (HRTEM, XPS, Raman and etc.) show that Ru/Co@NC possesses 2D structure with a high specific surface area, and the Ru successfully modified the Co surface to form a heterogeneous structure, which is beneficial to enhancement interaction between Ru and Co@NC. Electrochemical test results suggest that Ru/Co@NC possesses extraordinary HER activity with the low η that of 10, 283 and 50 mV at the current density (j) of 10 mA cm $^{-2}$ in 1.0 M KOH, 0.01 M PBS and 0.5 M H₂SO₄, respectively, compare favorably with benchmark Pt/C catalyst (26, 289 and 37 mV). Moreover, theoretical calculations show that the outstanding HER activity of Ru/Co@NC can be attributed to the interfacial electron interaction between Ru and Co (Co@NC).

2. Experimental section

2.1. Synthesis of NC and Co@NC

Firstly, a protonated g- C_3N_4 (P-g- C_3N_4) was prepared by thermal annealing of dicyandiamide and treatment of HCl (37 wt%). Then, 0.2 g of the as-prepared P-g- C_3N_4 were dispersed in 100 mL deionized water (DIW) under water bath ultrasonication for 0.5 h. And then, 0.2 mmol of $K_3Co(CN)_6$ was poured to the above solution under 5 min stirring. Next, 20 mL of $Co(NO_3)_2$ aqueous solution (7.5 mM) was added under stirring for 2 h. Subsequently, 0.5 mL of $NH_3\cdot H_2O$ (37 wt%) was dropped into the above solution under 5 min stirring. Next, an 20 mL aqueous solution containing 0.1 g of dopamine hydrochloride was added under 12 h stirring, and the precipitates were collected by suction filtration, washed with absolute ethanol for five times, and dried at 60 °C overnight. Finally, Co@NC was obtained by pyrolysis of the precipitates in an Ar atmosphere at 800 °C for 2 h. NC was synthesized by the alike method except for the addition of $K_3Co(CN)_6$ and $Co(NO_3)_2$.

2.2. Synthesis of Ru/Co@NC

40 mg of the as-prepared Co@NC were dispersed in 80 mL of DIW under ultrasonication to gain a homogeneously mixed solution, followed by adding 125, 150 or 175 μl of a RuCl $_3$ solution (40 mg mL $^{-1}$) under continuous 2 h stirring. The resulting dark products were collected, rinsed five times with DIW, and dried in an electric oven at 60 °C. Finally, the resulting products were heat treated at 300 °C in an Ar/H $_2$ atmosphere for 1 h, and named as Ru/Co@NC-125, Ru/Co@NC and Ru/Co@NC-175, respectively.

2.3. Synthesis of Ru/NC

40 mg as-prepared NC was dispersed in 80 mL DIW under ultrasonication to gain an mixed solution, followed to added 150 $\mu l~RuCl_3$ solution with 30 min stirring, then adding 10 mL NaBH4 solution into the above solution. Subsequently, the dark product was collected and rinsed several times with DIW dried under the electric oven at 60 °C. Then the resulting product was obtained by heat treating at 300 °C in an Ar/H2 atmosphere for 1 h.

2.4. Synthesis of NiFe-LDH

According to previous literature[33], 367.5 mg Ni(NO₃)₂, 170 mg Fe (NO₃)₃ and 9 g urea were dissolved in a homogeneous mixed solution of *N*-methylpyrrolidone (NMP) and H_2O , then the mixed solution was heated 100 °C for 6 h. Finally, the NiFe-LDH was collected by rinsing with ethanol and DIW and drying in the electric oven at 60 °C.

2.5. Characterization

Transmission electron microscopy (TEM) characterization was carried out on an S-4800, Hitachi and a Tecnai G2-F20 equipped with EDS, respectively. The crystalline phase was identified by X-ray diffraction (XRD) with a Bruker D8-Advance diffractometer. Raman spectra were recorded by using a LabRAM HR Evolution. X-ray photoelectron spectroscopy (XPS) were measured by Phi X-tool instrument. Thermogravimetric analysis (TGA) was measured by METTLER equipment in N₂. Brunauer-Emmet-Teller (BET) specific surface area and porous structure were measured by QuantachromeAutosorb-iQ-TPX.

2.6. Electrochemical measurements

Basic electrochemical tests were performed in the three-electrode system with the CHI 660D workstation in 1 M KOH electrolyte. A catalyst modified carbon cloth electrode (loading: 0.5 mg cm⁻²), a graphite rod and a standard Ag/AgCl electrode were used as the working, counter and reference electrodes, respectively. The Ag/AgCl electrode are converted to reversible hydrogen electrode through the equation: $E_{\text{RHE}} = E_{\text{SCE}} + 1.059 \text{ V}$. The homogeneous catalyst inks were prepared by 10 mg samples dispersed in 2 mL of a 3:1 V/V water/ ethanol mixed solvent (contains 40 μl 5 wt% Nafion). Linear sweep voltammetry (LSV) of HER was tested with a scan rate of 5 mV s⁻¹, and the potentials are corrected by the formula $E=E_{test}$ – iRs, in which the Rs is the solution impedance. The 20 wt% Pt catalyst with same loading was used as the reference sample. The electrochemical double-layer capacitance (C_{d1}) was probed by cyclic voltammetry (CV) from 0.1 -0.2 V vs RHE to reckon the electrochemical active area. Electrochemical impedance spectroscopy (EIS) were conducted at $j = 10 \text{ mA cm}^{-2}$ from 10,000 to 0.01 Hz. Current density-time (i-t) responses were monitored at j of about 10 mA cm⁻² for 30 h using a catalyst-modified carbon cloth. Accelerated decay tests (ADT) are carried out in the voltage range of 0 --0.2 V vs RHE. Overall water splitting measurements were measured by H-type dual electrode electrolyzer. The Ru/Co@NC and NiFe-LDH catalysts coated onto carbon cloth substrate (loading 1 mg cm⁻²) were applied as the cathode and anode, respectively.

2.7. Theoretical calculations

All theoretical calculations were performed within Density Functional Theory (DFT), and the electrocatalytic properties and electronic structure of prepared materials were investigated by using the CASTEP module in Materials Studio 2017. The the electronic exchange and correlation effects was described by generalized gradient approximation (GGA) with the Perdew-Burke-Ernzerhof (PBE) function, and the planewave cutoff was tested and stated to 500 eV. The self-consistent field (SCF) tolerance was 2 \times 10 $^{-6}$ eV with the ultrasoft pseudo-potential for

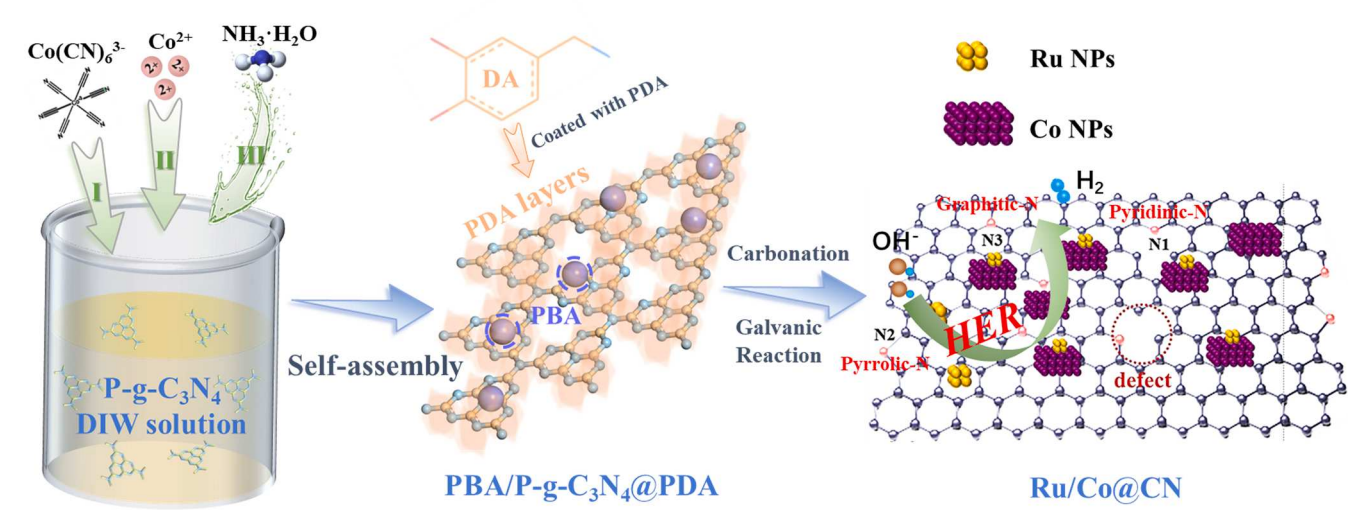


Fig. 1. Schematic illustration of the preparation of Ru/Co@NC.

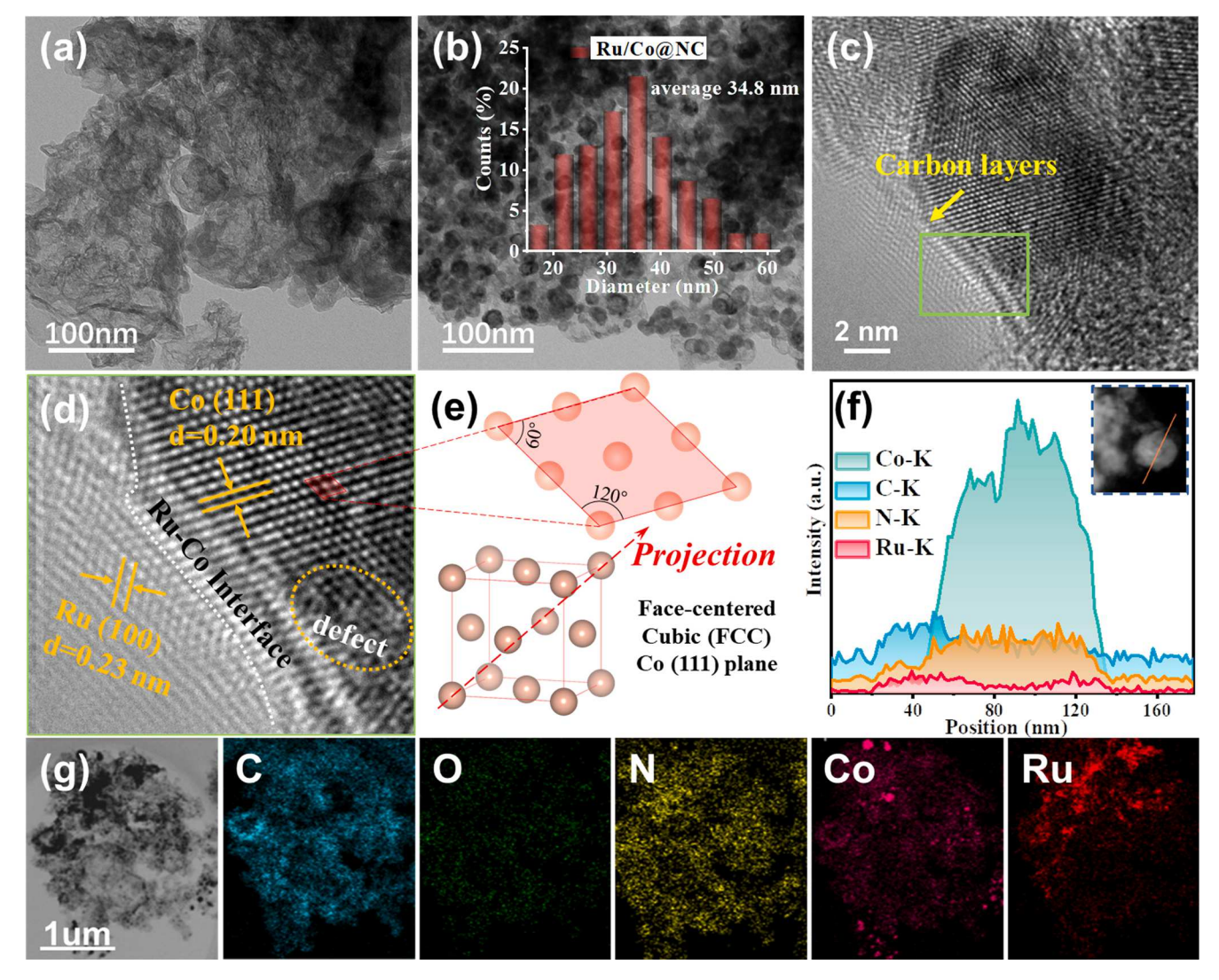


Fig. 2. (a-b) TEM images of NC and Ru/Co@NC, respectively. (Inset: the statistical particle size distribution pots) (c) HRTEM image of Ru/Co@NC, (d) Enlarged images showing grains individually and (e) Corresponding crystal structure diagram. (f) Line-scan profiles of Ru/Co@NC and the corresponding elemental curves. (g) STEM image and the corresponding elemental mapping of Ru/Co@NC.

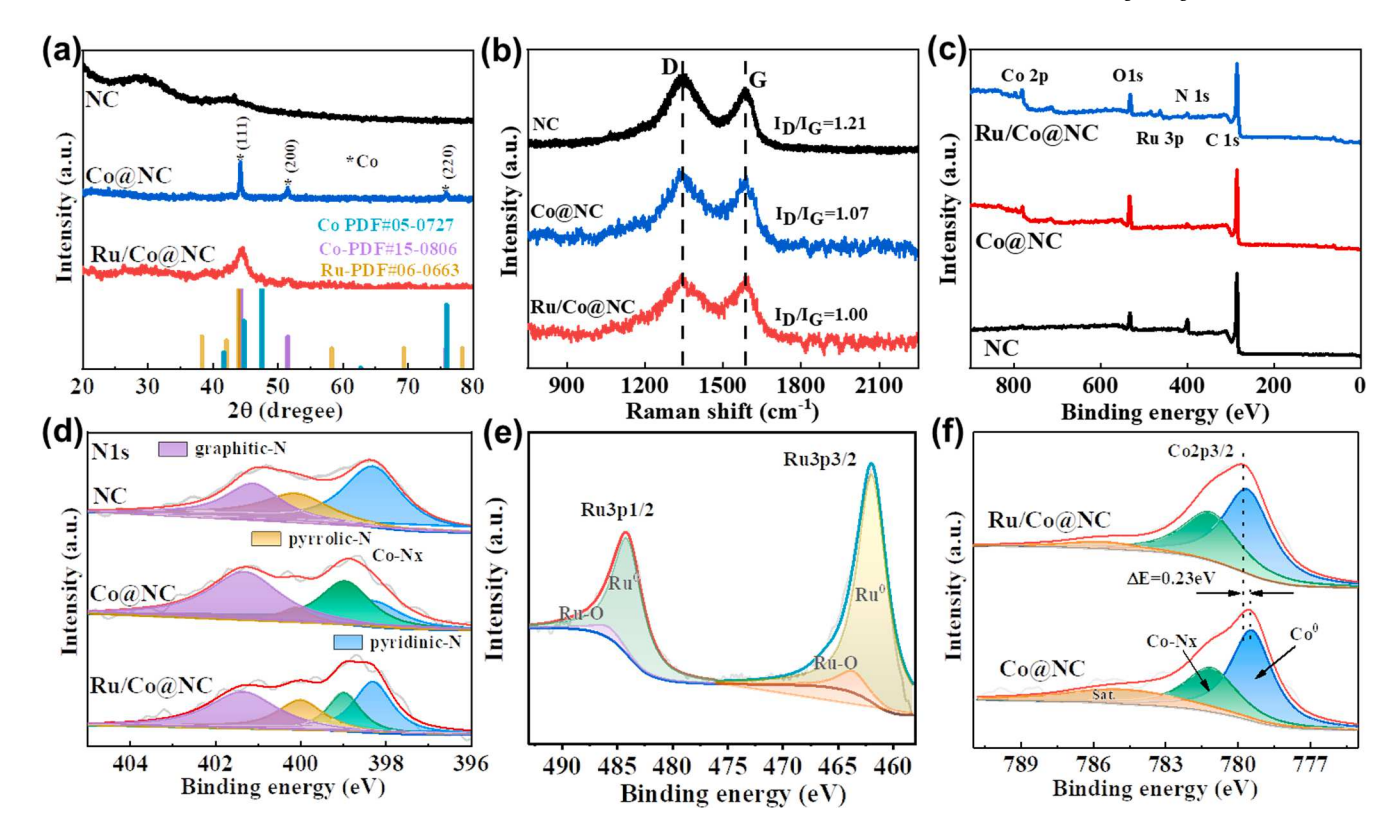


Fig. 3. (a) XRD patterns, (b) Raman spectra and (c) full XPS survey spectra of NC, Co@NC, and Ru/Co@NC. (d) High-resolution spectra of the N 1s of NC, Co@NC and Ru/Co@NC. (e) High-resolution spectra of the Ru 3p of Ru/Co@NC. (f) High-resolution spectra of the Co 2p of Co@NC and Ru/Co@NC.

core electrons.

3. Result and discussion

The synthesis process of Ru/Co@NC is shown in Fig. 1, the P-g-C₃N₄ is used as a 2D thermally removable template (completely decomposed at 700 °C as suggested from the TGA results depicted in Figure S1). Briefly, P-g-C₃N₄ is mixed with $[\text{Co(CN)}_6]^{3^-}$ and Co^{2^+} , PBAs are thus formed by self-assembly between Co^{2^+} and negatively charged $[\text{Co}(\text{CN})_6]^{3^-}$ adsorbed onto P-g-C₃N₄. Subsequently, a dopamine solution is added to generate polydopamine coating on PBA/P-g-C₃N₄, and annealing at a temperature over 700 °C leads to the formation of Co@NC. Finally, Ru/Co@NC is produced by galvanic replacement reaction between RuCl₃ and Co⁰ from Co@NC.

The morphology and structure of as-synthesized materials are performed by TEM. Fig. 2a and Figure S2a-c show that the NC presents a clear 2D sheet-like stacking structure. Compared to NC, there are some irregular nanoparticles (NPs) embedded in carbons sheets by seeing the TEM images of Co@NC (Figure S2d-e and Figure S3) and Ru/Co@NC (Fig. 2b), and the average particle sizes are about 61.0 and 34.8 nm, respectively. Moreover, some NPs of Ru/Co@NC display a hollow structure in comparison with Co@NC, which might be related to the Kirkendall effect during galvanic etching. In Figure S2f, the HRTEM image of Co@NC exhibits that defective carbon layers are uniformly coated on NPs surface, and the clear lattice fringes with lattice d-spacing of 0.204 nm is found, referring to face-centered cubic (fcc) Co (111) indicates the Co element in PBAs has been reduced to Co NPs by hightemperature annealing[34]. The HRTEM images for Ru/Co@NC are depicted in Fig. 2c-e, where the carbon layers and Co (111) can still be found, while the Co NPs possess some defects due to the etching of RuCl₃. Additionally, the clear new lattice fringes with a d-spacing 0.23 nm on the surface of Co NPs can be observed, which is assigned to the Ru (100) plane[35]. The HRTEM results confirm that the Ru successfully modified onto the surface of Co NPs, forming the Ru-Co heterostructure,

which is conducive to fully combine the advantages between Co and Ru and enhance the interaction between Co@NC and Ru.

The elemental distribution of Ru/Co@NC are then evaluated by linescanning curves. In Fig. 2f, Ru/Co@NC shows a typical core-shell structure, carbon layers are concentrated on the surface of sample clearly, while Co is in the interior, supporting the HRTEM results. According to the intensity of the diffraction peak, the Ru content in the sample is much less than that of Co. The elemental mapping images are depicted in Fig. 2g, where some Co and Ru elements display the agglomerate granular morphology, further indicating the existence of Co and Ru NPs in the samples. Moreover, the ratio of elements in the asprepared sample is estimated by EDS analysis (Figure S4a-c), the contents of C, N, O, Co and Ru in Ru/Co@NC are 72.47,3.46, 13.9, 8.48 and 1.69 at. %, respectively. In addition, ICP analysis (Table S1) is carried out to determine the metal content of the sample more accurately, in which the contents of Ru and Co in Ru/Co@NC are 2.3 and 36.23 wt%, respectively. All these facts support the formation of Ru decorated Co nanoparticles supported by N-doped carbon sheets.

The phase compositions and crystallinities are further characterized by XRD and Raman. From the XRD pattern (Fig. 3a), three peaks at about 44.2, 51.5, and 75.6° observed in Co@NC and Ru/Co@NC can be respectively directed to the (111), (200), and (220) planes of *fcc* Co (PDF card: 15–0806)[36], but no representative peaks about Ru can be observed from the pattern of Ru/Co@NC due to its low content in the material. As shown in Fig. 3b, Raman spectrum of as-prepared samples exhibits two broad peaks at 1350.0 and 1580.0 cm $^{-1}$, corresponding to the D (disordered) and G (graphite) band, respectively[37]. The ratio of the peak intensity of D and G (I_D/I_G) is applied to evaluate the graphitization of samples. The I_D/I_G of Ru/Co@NC and Co@NC are ca.1.00 and 1.07 lower than NC (ca. 1.27). This indicates that Ru/Co@NC and Co@NC have similar carbon-based structures, the introduction of Ru only slightly reduced the graphitization degree of the catalyst.

The specific surface areas (SSA) for different samples are evaluated via N₂ adsorption–desorption isotherms (Figure S5a), NC exhibits the

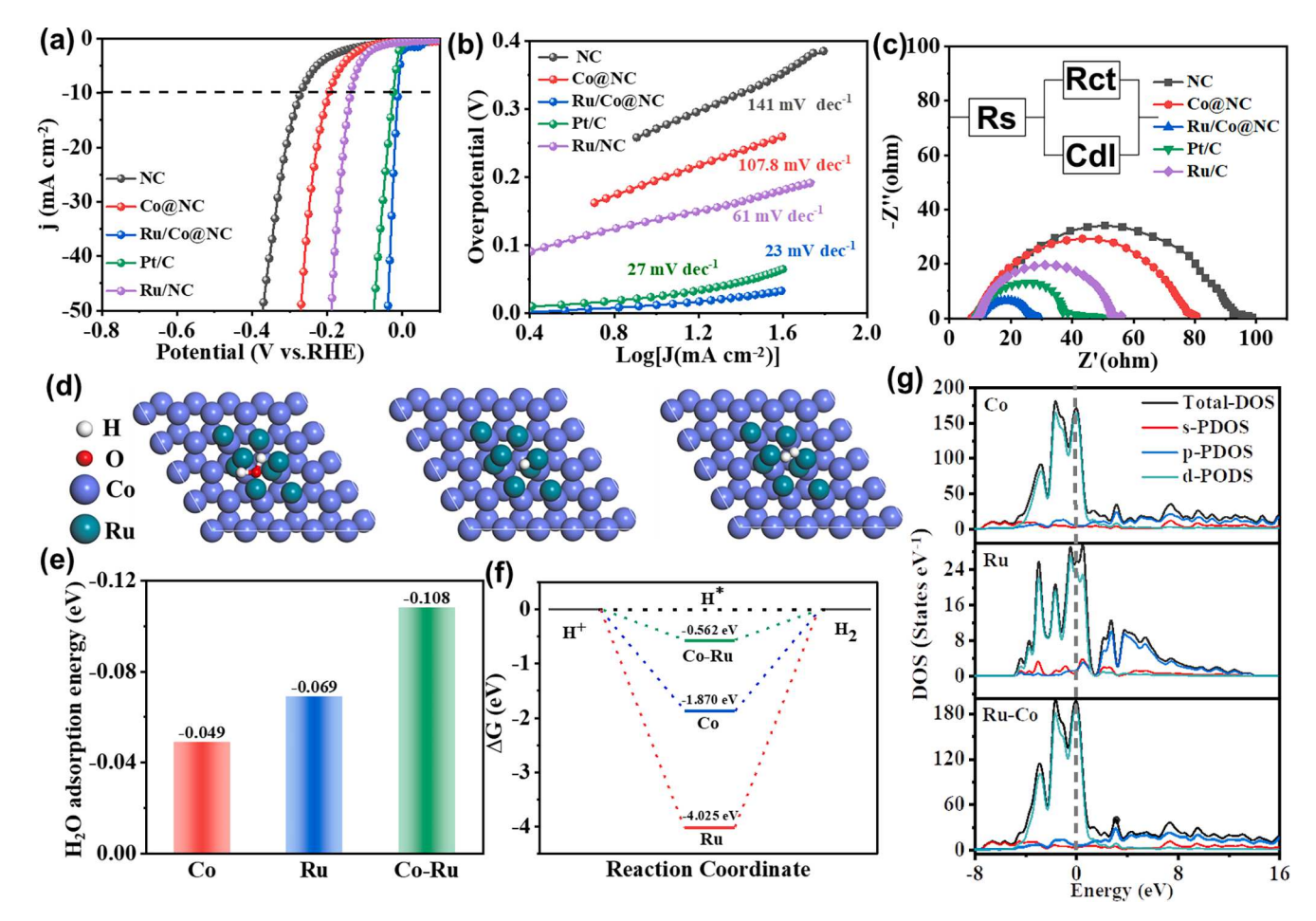


Fig. 4. (a) LSV curves with iR-correction, (b) Tafel plots and (c) Nyquist plots for HER in 1.0 M KOH of as-prepared samples and Pt/C. (d) Top-view schematic models of Co-Ru heterostructures with H* and H₂O adsorbed on the surface, respectively. (e) H₂O adsorption energy on the surfaces and (f) DFT-calculated free-energy change for HER of Co-Ru heterostructures, Ru, and Co. (g) The density of states (DOS) of Ru-Co heterostructure, single Ru and Co.

highest SSA of 505 m² g⁻¹ among all samples. The SSA of Co@NC decreases to 281 m² g⁻¹ because of the formation of Co NPs in the pores of the carbon substrate. The SSA of Ru/Co@NC (267 m² g⁻¹) is close to Co@NC. **Figure S5b** shows the pore size distribution, where the pore size for NC, Co@NC and Ru/Co@NC mainly ranges from 2 to 55 nm, belonging to mesoporous. The average pore size can be seen to decrease after Co NPs loading (Co@NC = 13.14 nm) on NC (NC = 22.31 nm), and remain unchanged during Ru replacement (Ru/Co@NC = 13.05 nm). Similarly, the average pore volume value is 1.76 cm³ g⁻¹ for NC, 0.76 cm³ g⁻¹ for Co@NC and 0.74 cm³ g⁻¹ for Ru/Co@NC. Above results suggests that the SSA and pore volume are almost unchanged before and after the Ru-decoration. To sum up, the outstanding SSA, pore volume and diameter distribution of as-prepared catalysts are beneficial to mass transfer in the HER process[38].

Furthermore, the XPS analysis is measured to investigate the valence states of as-prepared samples. In Fig. 3c, five peaks can be resolved at 285, 400, 475, 534, and 780 eV in the full XPS spectrum of Ru/Co@NC, which are ascribed to the C 1 s, N 1 s, O 1 s, Co 2p and Ru 3p, respectively. According to the integrated peak areas, the contents are estimated to be 76.20, 5.81, 13.81, 3.10 and 1.08 at. %, very close to the EDS results. Figure S6 demonstrates the C 1 s spectra of the different materials, the deconvoluted peaks located at about 284.6, 285.6 and 288.1 eV correspond to the C=C, C=N/C=O and C=O/C=N[39]. Moreover, the weak peak at 280.5 eV belongs to Ru 3d5/2. From the N 1 s spectra for Ru/Co@NC (Fig. 3d), the four peaks can be divided, which are assigned to pyridinic-N (398.3 eV), Co-Nx (399.0 eV), pyrrolic-N (400.1 eV) and graphitic-N (401.3 eV)[40,41], exhibiting that N and Co elements were indeed successfully doped into the carbon substrate.

Additionally, deconvolution of the Ru 3p spectrum (Fig. 3e) yields two distinct peaks around 463.0 and 485.0 eV, corresponding to Ru⁰[42], consistent with the TEM. Moreover, due to exposure to air, there is a small amount of Ru-O on the surface of Ru/Co@NC. In Fig. 3f, the Co 2p spectra can be divided into three peaks, metallic Co (779.0 eV), Co-Nx (781.3 eV) and satellite peak (786.0 eV)[43]. Moreover, the binding energy of Co 2p3/2 in Ru/Co@NC shows a positive shift of about 0.23 eV, as compared to that of Co@NC, indicating electron transfer from Co (1.9) to Ru (2.2) because of the difference in electronegativity, which demonstrates the interaction between Co@NC and Ru.

The HER performances are first investigated by electrochemical measurements in 1.0 M KOH. In Figure S7, Ru/Co@NC catalysts synthesized by controlling Ru loading all show remarkable catalytic activity for HER. In LSV curves (Fig. 4a), the Ru/Co@NC exhibits the best HER activity among all as-prepared catalysts and even surpasses Pt/C, the η_{10} of Ru/Co@NC is as low as 10 mV at j of 10 mA cm $^{-2}$, much better than these of NC (ca. 273 mV), Co@NC (ca. 194 mV), Ru/NC (ca. 130 mV), and Pt/C (ca. 26 mV) catalyst (Figure S8). In addition, the Tafel slope (derived from LSV results and concluded in Fig. 4b) of Ru/Co@NC is as low as 23 mV dec $^{-1}$. Such a value is much smaller than homemade samples obtained on the reference and Pt/C catalysts (27 mV dec $^{-1}$). The results indicate that the synergistic effect of Ru and Co@NC is beneficial to enhance the kinetics of the Volmer reaction during the HER process [441].

The C_{dl} and EIS are then performed to better study the enhanced HER activity on Ru/Co@NC. The C_{dl} is probed by CV at non-faradaic potential range, the CV curves of as-prepared samples exhibited in Figure S9a-c. In the corresponding C_{dl} plots (Figure S9d), the Ru/

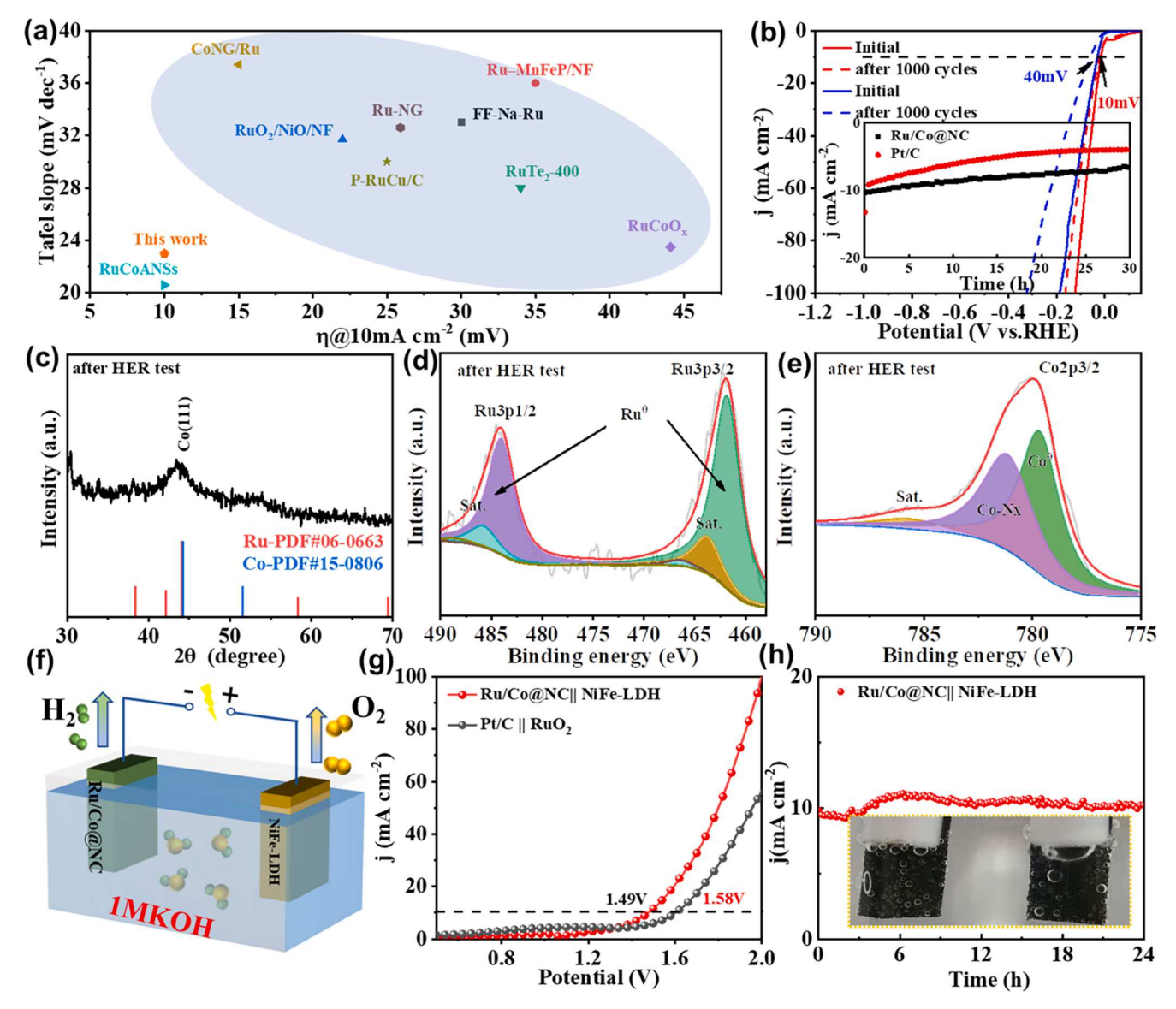


Fig. 5. (a) The correlation plot between overpotential and Tafel slope at j_{10} of Ru/Co@NC and different materials from previous literature. (b) The LSV and i-t (inserted) curves before and after 1000th CV test. (c, d and e) The XRD patterns, Ru 3p and Co 2p3/2 spectra of Ru/Co@NC after long-time HER test. (f) Schematic model of a water electrolyzer. (g) The LSV and (h) i-t curves (around j_{10}) of overall water splitting for Ru/Co@NC || NiFe-LDH in 1.0 M KOH.

Co@NC shows the highest $C_{\rm dl}$ (ca. 100.1 mF cm $^{-2}$) among the sample series, which implies the highest ECSA on Ru/Co@NC. Moreover, the LSVs normalized by ECSA (Figure \$10) shows that Ru/Co@NC have the best intrinsic activity among all as-prepared samples. In the Nyquist plots and equivalent circuit diagram (Fig. 4c), Rct represents the electron-transfer resistance from the electrolyte to the electrocatalyst surface, which was relevant to reaction kinetics of the sample. The lower R_{ct} indicates the faster kinetics, which can be evaluated by a semicircle of Nyquist plots in the low-frequency range. Among all catalysts, the Ru/ Co@NC exhibits the lowest R_{ct} of ca. 20 for HER, which is suggesting the most efficient electron transfer, thus Ru/Co@NC obtains the most outstanding HER activity among all as-prepared samples. The Faradaic efficiency (FE) was calculated by using the chronopotentiometric reaction at $j = 10 \text{ mA cm}^{-2}$ (Figure S11), the amount of hydrogen produced at different times is recorded can gas chromatography, the FE is close to 100 %. All above electrochemical tests show that Ru/Co@NC exhibits excellent catalytic activity for HER.

Furthermore, the DFT calculation is a proven and effective method to study reasons of the outstanding HER activity of Ru/Co@NC, and the structural model of Ru, Co (111), Ru-Co (111) could be depicted in

Figure S12. In alkaline media, the HER mechanism of Ru/Co@NC follows the Volmer-Tafel steps[45]:

Volmer process: $H_2O + * + e^- \leftrightarrow OH^- + H^*$.

Tafel process: $2H^* \leftrightarrow H_2$.

The corresponding adsorption models with H_2O^* , H^* and H_2^* molecule on the surface is displayed in Fig. 4d and Figure S13a-b. As shown in Fig. 4e, the Ru-Co heterostructure displays the lowest H_2O adsorption energy (-0.108 eV), in comparison to Ru (-0.069 eV) and Co (-0.049 eV), demonstrating that H_2O can be easily formed on the surface of Ru-Co heterostructure material to form H_2O^* , which facilitates H_2O dissociation greatly [46]. Moreover, it is well-known that the Gibbs freeenergy of H^* (ΔG_H^*) can serve as evaluation parameter on the HER activity (the smaller $|\Delta G_H^*|$ enables a better activity toward HER)[47]. Fig. 4f shows the ΔG_H^* of Ru-Co heterostructure, single Ru and Co. The ΔG_H^* of Ru-Co heterostructure is -0.562 eV, much smaller than Ru (-4.025 eV) and Co (-1.870 eV). This result demonstrates the more favorable H^* adsorption kinetics on Ru-Co heterostructure, consistent with the significantly improved HER performance observed in the experiment.

In addition, the continuous distribution of the DOS for Ru, Co and

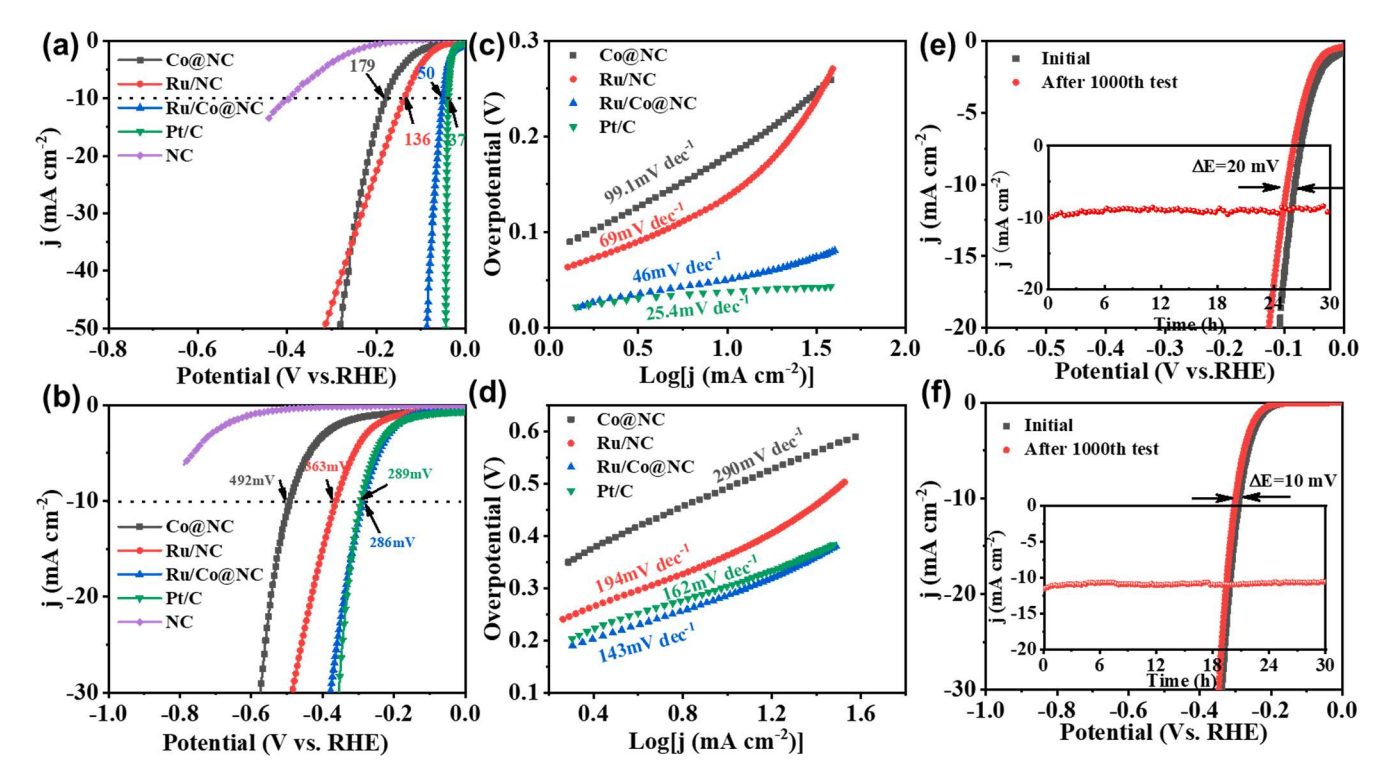


Fig. 6. (a-b) HER LSVs, (c-d) The corresponding Tafel plots of as-prepared samples and (e-f) The LSV curves for Ru/Co@NC before and after 1000th CV test (Inset: the i-t curves of Ru/Co@NC) in 0.5 M $_{12}$ SO₄ and 0.01 M PBS (pH = 7.4).

Ru-Co are near the Fermi level (Fig. 4g), indicating the catalytic site in a metallic state with high conductivity. This favors fast electron transfer during the electrochemical process. Indeed, the more electron states exist around the Fermi level, the higher electronic conductivity of the catalysts [48]. The unique electronic structure around the Fermi level ensured that the Ru-Co heterostructure exhibited higher electronic conductivity and better electrocatalytic activity than that of the single Ru and Co. The PDOS further evaluated the interaction between Ru and Co in the heterostructure catalyst. The calculation indicated the remarkable electrical conductivity and fast electron transport in Ru-Co heterostructure catalyst, favoring the electrocatalytic HER. Moreover, the surface charge density analysis (Figure S14a, b), the surface charge density of Co (111)/Ru is redistributed compared to Co (111), which achieves an obvious electron accumulation on Ru site, further indicate that Co can effectively regulates the electronic structure of Ru, agreement with the XPS results. Previous studies have been proved that the electron-rich Ru sites produced by the localized structural polarization can reduced energy barrier of water dissociation, thus the Ru/Co@NC exhibits the better HER activity than that of Ru/NC.

Combining DFT and electrochemical test results, we can conclude that Ru/Co@NC exhibits the excellent HER activity in 1.0 M KOH, comparable to the most advanced Ru-based materials reported in literature (Fig. 5a)[18,23,49–56]. Besides activity, stability is also a crucial parameter for electrocatalysts, which can be evaluated through the i-t and accelerated attenuation test (ADT). In Fig. 5b, one can find that Ru/Co@NC shows good HER stability, there is a negative potential shift of ca. 10.0 mV at j₁₀ after ADT, whereas Pt/C has a much larger negative shift of ca. 40 mV. In addition, it can be seen that ca. 70 % of the j was retained with Ru/Co@NC after 30 h continuous operation at j₁₀, in comparison to only ca. 50 % on Pt/C (Fig. 5a inset). These results strongly confirm the outstanding durability of Ru/Co@NC, exceeding the performance of Pt/C.

To further analyze the reasons of the high HER stability, the morphology, structure and oxidation state of Ru/Co@NC after i-t test for HER have been characterized by TEM, XRD and XPS. The TEM images (Figure \$15a-b) exhibit that the morphology and structure of Ru/

Co@NC are barely changed except for a slight increase of the NP size after the HER test, the Co (111) and Ru (100) planes still can be observed. These facts are in good agreement with XRD and XPS analysis. As shown in Fig. 5c, the XRD characteristic diffraction peak of Co (111) can be retained in the Ru/Co@NC. Moreover, the peaks of Ru 0 and Co 0 still can be observed after long-time HER test in Fig. 5d-e. These results reflect a fact that the Ru/Co@NC can keep the good structure and morphology after long-time HER test, thus demonstrating excellent catalyst stability.

Due to outstanding HER activity and durability, Ru/Co@NC is expected to be a potential catalyst for water electrolyzer (the corresponding model shown in Fig. 5f), which united with a good OER catalyst can realize efficient overall water splitting (OWS). Herein, we synthesize a NiFe-LDH material that is one of the popular transition-metal OER catalysts, and as-made NiFe-LDH possesses high OER performance ($\eta_{10}=280$ mV) than that of commercial RuO2 (300 mV) (Figure S16). The LSV curves for OWS are shown in Fig. 5g, in which the Ru/Co@NC || NiFe-LDH coupes electrode shows that a low total voltage of only 1.49 V is required to achieve j_{10} , markedly smaller than that with a Pt/C + RuO2 mixed catalysts (1.58 V). The i-t measurement for stability on Ru/Co@NC || NiFe-LDH at 1.50 V is shown in Fig. 5h. After 24 h continuous operation, no apparent attenuation of j can be recorded, suggesting that practice electrolysis of water application prospects of Ru/Co@NC.

Unsurprisingly, the Ru/Co@NC also displays superior HER catalytic ability in both the acidic and neutral electrolytes by reason of the appropriate $\rm H_2O$ and H adsorption energy. As exhibited in Fig. 6a-b and Figure S17, the η of Ru/Co@NC at j_{10} are only 50 and 286 mV, respectively, which are lower than that of NC (393 and > 700 mV), Co@NC (179 and 492 mV) and Ru/NC (136 and 363 mV), and even comparable to Pt/C (37 and 289 mV). The corresponding Tafel plots are exhibited in Fig. 6c-d, Ru/Co@NC shows Tafel slopes of 46 and 143 mV dec $^{-1}$ in 0.5 M KOH and 0.01 M PBS, outperforming that of Co@NC (99.1 and 290 mV dec $^{-1}$) and Ru/NC (69 and 194 mV dec $^{-1}$), indicating that the fastest HER kinetics among all as-prepared samples.

Moreover, Ru/Co@NC displays the higher mass activity (10, 3.0 and

 $2~A~mg^{-1})$ than that of Pt/C (0.34, 0.23 and $1~A~mg^{-1})$ in 1~M KOH, 0.01 M PBS and $0.5~H_2{\rm SO}_4$ solution, respectively (Figure S18), comparable to some advanced precious metal HER catalyst[23,56–58]. Fig. 6e-6f show that Ru/Co@NC exhibits high HER stability in acidic and neutral electrolytes as well, the η_{10} of Ru/Co@NC only increases 20 and 10 mV in 0.5 M KOH and 0.01 M PBS, respectively. The long-time durability of Ru/Co@NC displays a slight decay in j after 30 h water electrolysis. The above results demonstrate that Ru/Co@NC shows good HER performances and stabilities in a wide pH range.

4. Conclusion

In conclusion, we have successfully prepared Ru decorated Co nanoparticles supported by N-doped carbon sheet (Ru/Co@NC) via the galvanic exchange reaction. The Ru/Co@NC displays Pt-like electrocatalytic activity for HER with the ultralow $\eta_{10}\,(10,283\,\text{and}\,50\,\text{mV})$ and small Tafel slopes (24, 143 and 46 mV dec⁻¹) in 1.0 M KOH, 0.01 M PBS and 0.5 M H₂SO₄, respectively. Additionally, Ru/Co@NC also shows excellent HER stability with no significant performance attenuation after 30 h HER test at the wide pH range. Based on experimental and theoretical results, the remarkable activity and stability stem from the following three points: one is the Co-Ru heterostructure can enhance the strong interaction between Co@NC and Ru and modulate each other's electronic structures, which is beneficial to accelerate the dissociation of water and the absorption/desorption of H* and thus boost the electrocatalytic performance. Other is the 2D Co@NC substrate with high electrical conductivity and large specific surface area to enhance the mass/electron transfer during the reaction process.

Declaration of Competing Interest

The authors declare that they have no known competing financial interests or personal relationships that could have appeared to influence the work reported in this paper.

Data availability

Data will be made available on request.

Acknowledgments

This work was supported by the Natural Science Foundation of Guangdong Province, China (2019A1515011727); the Fundamental Research Funds for the Central Universities (21620329); the Post-doctoral Research Foundation of China (2020M673071); the Open Fund of the Guangdong Provincial Key Laboratory of Advance Energy Storage Materials; the Science and Technology Planning Project of Guangzhou, China (201605030008) and the National Innovation and Entrepreneurship Training Program for Undergraduate (202110559044). S.W.C. thanks the National Science Foundation for partial support of the work (CHE-1900235 and CHE-2003685).

Appendix A. Supplementary data

Supplementary data to this article can be found online at https://doi. org/10.1016/j.cej.2022.138254.

References

- [1] J. Zhu, L. Hu, P. Zhao, L.Y.S. Lee, K.-Y. Wong, Chem. Rev. 120 (2020) 851–918.
- [2] Y. Jiao, Y. Zheng, M. Jaroniec, S.Z. Qiao, Chem. Soc. Rev. 44 (2015) 2060–2086.
- [3] H. Lu, J. Tournet, K. Dastafkan, Y. Liu, Y.H. Ng, S.K. Karuturi, C. Zhao, Z. Yin, Chem. Rev. 121 (2021) 10271–10366.
- [4] L. Han, S. Dong, E. Wang, Adv. Mater. 28 (2016) 9266–9291.
- [5] Y. Li, X. Zhang, S. Zhuo, S. Liu, A. Han, L. Li, Y. Tian, Appl. Surf. Sci. 555 (2021), 149441.
- [6] J.N. Tiwari, N.K. Dang, S. Sultan, P. Thangavel, H.Y. Jeong, K.S. Kim, Nat. Sustain. 3 (2020) 556–563.

- [7] P. Thangavel, M. Ha, S. Kumaraguru, A. Meena, A.N. Singh, A.M. Harzandi, K. S. Kim, Energy Environ. Sci. 13 (2020) 3447–3458.
- [8] A.M. Harzandi, S. Shadman, A.S. Nissimagoudar, D.Y. Kim, H.-D. Lim, J.H. Lee, M. G. Kim, H.Y. Jeong, Y. Kim, K.S. Kim, Adv. Energy Mater. 11 (2021) 2003448.
- [9] P. Thangavel, G. Kim, K.S. Kim, J. Mater. Chem. A 9 (2021) 14043–14051.
- [10] N.K. Dang, J.N. Tiwari, S. Sultan, A. Meena, K.S. Kim, Chem. Eng. J. 404 (2021), 126513.
- [11] Y. Wang, H. Su, Y. He, L. Li, S. Zhu, H. Shen, P. Xie, X. Fu, G. Zhou, C. Feng, D. Zhao, F. Xiao, X. Zhu, Y. Zeng, M. Shao, S. Chen, G. Wu, J. Zeng, C. Wang, Chem. Rev. 120 (2020) 12217–12314.
- [12] Z. Cheng, Y. Xiao, W. Wu, X. Zhang, Q. Fu, Y. Zhao, L. Qu, ACS Nano 15 (2021) 11417–11427.
- [13] Y. Liu, X. Liu, X. Wang, H. Ning, T. Yang, J. Yu, A. Kumar, Y. Luo, H. Wang, L. Wang, J. Lee, A.R. Jadhav, H. Hu, M. Wu, M.G. Kim, H. Lee, ACS Nano 15 (2021) 15017–15026.
- [14] D. Reynard, B. Nagar, H. Girault, ACS Catal. 11 (2021) 5865-5872.
- [15] W. He, X. Zheng, J. Peng, H. Dong, J. Wang, W. Zhao, Chem. Eng. J. 396 (2020), 125227.
- [16] M. Luo, S. Liu, W. Zhu, G. Ye, J. Wang, Z. He, Chem. Eng. J. 428 (2022), 131055.
- [17] J. Su, Y. Yang, G. Xia, J. Chen, P. Jiang, Q. Chen, Nat. Commun. 8 (2017) 14969.
- [18] Q. Qin, H. Jang, L. Chen, G. Nam, X. Liu, J. Cho, Adv. Energy Mater. 8 (2018) 1801478
- [19] Q. Wu, M. Luo, J. Han, W. Peng, Y. Zhao, D. Chen, M. Peng, J. Liu, F.M.F. de Groot, Y. Tan, ACS Energy Lett. 5 (2020) 192–199.
- [20] J.N. Tiwari, A.M. Harzandi, M. Ha, S. Sultan, C.W. Myung, H.J. Park, D.Y. Kim, P. Thangavel, A.N. Singh, P. Sharma, S.S. Chandrasekaran, F. Salehnia, J.-W. Jang, H.S. Shin, Z. Lee, K.S. Kim, Adv. Energy Mater. 9 (2019) 1900931.
- [21] N.K. Dang, M. Umer, P. Thangavel, S. Sultan, J.N. Tiwari, J.H. Lee, M.G. Kim, K. S. Kim, J. Mater. Chem. A 9 (2021) 16898–16905.
- [22] Y. Yang, J. Kim, C. Kim, A. Seong, O. Kwon, J.H. Lee, I. Kristanto, L. Zhang, J. Zhou, J.-Q. Wang, J.-B. Baek, S.K. Kwak, G. Kim, Nano Energy 76 (2020), 105114.
- [23] Y. Li, Y. Luo, Z. Zhang, Q. Yu, C. Li, Q. Zhang, Z. Zheng, H. Liu, B. Liu, S. Dou, Carbon 183 (2021) 362–367.
- [24] Y. Zheng, Y. Jiao, Y. Zhu, L.H. Li, Y. Han, Y. Chen, M. Jaroniec, S.-Z. Qiao, J. Am. Chem. Soc. 138 (2016) 16174–16181.
- [25] X. Wu, B. Feng, W. Li, Y. Niu, Y. Yu, S. Lu, C. Zhong, P. Liu, Z. Tian, L. Chen, W. Hu, C.M. Li, Nano Energy 62 (2019) 117–126.
- [26] Y. Liu, X. Li, Q. Zhang, W. Li, Y. Xie, H. Liu, L. Shang, Z. Liu, Z. Chen, L. Gu, Z. Tang, T. Zhang, S. Lu, Angew. Chem. Int. Ed. 59 (2020) 1718–1726.
- [27] M. Chen, Z. Fan, L. Ai, J. Jiang, Appl. Surf. Sci. 564 (2021), 150478.
- [28] H. Gao, J. Zang, X. Liu, Y. Wang, P. Tian, S. Zhou, S. Song, P. Chen, W. Li, Appl. Surf. Sci. 494 (2019) 101–110.
- [29] H. Wang, M. Zhou, X. Bo, L. Guo, Electrochim. Acta 382 (2021), 138337.
- [30] J. Jiao, N.-N. Zhang, C. Zhang, N. Sun, Y. Pan, C. Chen, J. Li, M. Tan, R. Cui, Z. Shi, J. Zhang, H. Xiao, T. Lu, Adv. Sci. 9 (2022) 2200010.
- [31] R. Kumar, E. Joanni, R.K. Singh, D.P. Singh, S.A. Moshkalev, Prog. Energy Combust. Sci. 67 (2018) 115–157.
- [32] Y. Hou, S. Cui, Z. Wen, X. Guo, X. Feng, J. Chen, Small 11 (2015) 5940-5948.
- [33] Q. Wang, L. Shang, R. Shi, X. Zhang, Y. Zhao, G.I.N. Waterhouse, L.-Z. Wu, C.-H. Tung, T. Zhang, Adv. Energy Mater. 7 (2017) 1700467.
- [34] J. Zhao, X. Quan, S. Chen, Y. Liu, H. Yu, ACS Appl. Mater. Inter. 9 (2017) 28685–28694.
- [35] N. Wang, S. Ning, X. Yu, D. Chen, Z. Li, J. Xu, H. Meng, D. Zhao, L. Li, Q. Liu, B. Lu, S. Chen, Appl. Catal. B: Environ. 302 (2022), 120838.
- [36] C. Deng, K.-H. Wu, J. Scott, S. Zhu, X. Zheng, R. Amal, D.-W. Wang, ACS appl. mater. inter. 11 (2019) 9925–9933.
- [37] I.S. Amiinu, Z. Pu, X. Liu, K.A. Owusu, H.G.R. Monestel, F.O. Boakye, H. Zhang, S. Mu, Adv. Funct. Mater. 27 (2017) 1702300.
- [38] S.H. Lee, J. Kim, D.Y. Chung, J.M. Yoo, H.S. Lee, M.J. Kim, B.S. Mun, S.G. Kwon, Y.-E. Sung, T. Hyeon, J. Am. Chem. Soc. 141 (2019) 2035–2045.
- [39] D.C. Nguyen, D.T. Tran, T.L. Luyen Doan, N.H. Kim, J.H. Lee, Chem. Mater. 31 (2019) 2892–2904.
- [40] W. Niu, Z. Li, K. Marcus, L. Zhou, Y. Li, R. Ye, K. Liang, Y. Yang, Adv. Energy Mater. 8 (2018) 1701642.
- [41] W. Niu, S. Pakhira, K. Marcus, Z. Li, J.L. Mendoza-Cortes, Y. Yang, Adv. Energy Mater.
- [42] C. Cheng, S.S.A. Shah, T. Najam, X. Qi, Z. Wei, Electrochim. Acta 260 (2018) 358–364.
 [43] L. Wang, Z. Tang, Y. Wei, Q. Wang, H. Yang, S. Chen, J. Power Sources 343 (2017)
- 458–466. [44] Q. He, D. Tian, H. Jiang, D. Cao, S. Wei, D. Liu, P. Song, Y. Lin, L. Song, Adv. Mater.
- 32 (2020) 1906972. [45] Y. Shi, B. Zhang, Chem. Soc. Rev. 45 (2016) 1529–1541.
- [46] M. Zhou, H. Li, A. Long, B. Zhou, F. Lu, F. Zhang, F. Zhan, Z. Zhang, W. Xie, X. Zeng, D. Yi, X. Wang, Adv. Energy Mater. 11 (2021) 2101789.
- [47] Y. Zheng, Y. Jiao, Y. Zhu, L.H. Li, Y. Han, Y. Chen, A. Du, M. Jaroniec, S.Z. Qiao, Nat. Commun. 5 (2014) 3783.
- [48] Y. Gu, A. Wu, Y. Jiao, H. Zheng, X. Wang, Y. Xie, L. Wang, C. Tian, H. Fu, Angew. Chem. Int. Ed. 60 (2021) 6673–6681.
- [49] Z. Wu, Y. Zhao, H. Wu, Y. Gao, Z. Chen, W. Jin, J. Wang, T. Ma, L. Wang, Adv. Funct. Mater. 31 (2021) 2010437.
- [50] D. Chen, Z. Pu, R. Lu, P. Ji, P. Wang, J. Zhu, C. Lin, H.-W. Li, X. Zhou, Z. Hu, F. Xia, J. Wu, S. Mu, Adv. Energy Mater. 10 (2020) 2000814.
- [51] J. Liu, Y. Zheng, Y. Jiao, Z. Wang, Z. Lu, A. Vasileff, S.-Z. Qiao, Small 14 (2018) 1704073.

- [52] B. Tang, X. Yang, Z. Kang, L. Feng, Appl. Catal. B: Environ. 278 (2020), 119281.
 [53] C. Wang, L. Qi, Angew. Chem. Int. Ed. 59 (2020) 17219–17224.
 [54] C.-B. Hong, X. Li, W.-B. Wei, X.-T. Wu, Q.-L. Zhu, Appl. Catal. B: Environ. 294 (2021), 120230.
- [55] C. Cai, K. Liu, Y. Zhu, P. Li, Q. Wang, B. Liu, S. Chen, H. Li, L. Zhu, H. Li, J. Fu, Y. Chen, E. Pensa, J. Hu, Y.-R. Lu, T.-S. Chan, E. Cortés, M. Liu, Angew. Chem. Int. Ed. 61 (2022) e202113664.
- [56] T. He, Y. Peng, Q. Li, J.E. Lu, Q. Liu, R. Mercado, Y. Chen, F. Nichols, Y. Zhang, S. Chen, A.C.S. Appl, Mater. Inter. 11 (2019) 46912-46919.
- [57] A.M. Harzandi, S. Shadman, M. Ha, C.W. Myung, D.Y. Kim, H.J. Park, S. Sultan, W.-S. Noh, W. Lee, P. Thangavel, W.J. Byun, S.-H. Lee, J.N. Tiwari, T.J. Shin, J.-H. Park, Z. Lee, J.S. Lee, K.S. Kim, Appl. Catal. B: Environ. 270 (2020), 118896.
- [58] H. Zhang, H. Su, M.A. Soldatov, Y. Li, X. Zhao, M. Liu, W. Zhou, X. Zhang, X. Sun, Y. Xu, P. Yao, S. Wei, Q. Liu, Small 17 (2021) 2105231.